

Time-varying drainage basin development and erosion on volcanic edifices

Daniel O'Hara^{1,2}, Liran Goren³, Roos M.J. van Wees¹, Benjamin Campforts⁴, Pablo Grosse^{5,6}, Pierre Lahitte⁷, Gabor Kereszturi⁸, Matthieu Kervyn¹

¹Department of Geography, Vrije Universiteit Brussel, Pleinlaan 2, 1050 Elsene.

²Helmholz Center Potsdam, GFZ German Research Center for Geosciences, Potsdam, Germany.

³ Ben Gurion University of the Negev, Department of Earth and Environmental Sciences, Beer-Sheva, Israel

⁴Institute of Arctic and Alpine Research, University of Colorado Boulder, Boulder, CO, USA

⁵ Consejo Nacional de Investigaciones Científicas y Técnicas (CONICET), Argentina

⁶ Fundación Miguel Lillo, Miguel Lillo 251, (4000) Tucumán, Argentina

⁷ Université Paris-Saclay, CNRS, Laboratoire GEOPS, Rue du Belvédère, 91405 Orsay, France

⁸ Volcanic Risk Solutions, School of Agriculture and Environment, Massey University, 4474, New Zealand

Correspondence to: Daniel O'Hara (Daniel.OHara@vub.be)

Abstract. The erosional state of a landscape is often assessed through a series of metrics that quantify the morphology of drainage basins and divides. Such metrics have been well-explored in tectonically-active environments to evaluate the role of different processes in sculpting topography, yet relatively few works have applied these analyses to radial landforms such as volcanoes. We quantify drainage basin geometries on volcanic edifices of varying ages using common metrics (e.g., Hack's Law, drainage density, number of basins that reach the edifice summit, as well as basin hypsometry integral, length, width, relief, and average topographic slope). Relating these measurements to the log-mean age of activity for each edifice, we find that drainage density, basin hypsometry, basin length, and basin width quantify the degree of erosional maturity for these landforms. We also explore edifice drainage basin growth and competition by conducting a divide mobility analysis on the volcanoes, finding that young volcanoes are characterized by nearly-uniform fluvial basins within unstable configurations that are more prone to divide migration. As basins on young volcanoes erode, they become less uniform but adapt to a more stable configuration with less divide migration. Finally, we analyze basin spatial geometries and outlet spacing on edifices, discovering an evolution in radial basin configurations that differ from typical linear mountain ranges. From these, we present a novel conceptual model for edifice degradation that allows new interpretations of composite volcano histories and provides predictive quantities for edifice morphologic evolution.

1.0 Introduction

Understanding how drainage basins on eroding landforms develop and evolve is a fundamental principle of Geomorphology. Over regional scales, basin geometry, structure, and spacing evolve in response to both external (e.g., climate, tectonics; Castelltort et al., 2012; Duvall and Tucker, 2015; Han et al., 2015; Yang et al., 2015) and internal (e.g., channel piracy; Bishop, 1995; Whipple et al., 2016) forcing as topographic slopes adjust to develop and maintain an equilibrium between erosion and uplift (e.g., Willett et al., 2001; Castelltort et al., 2009). As these landscapes adjust, transient signals within basins propagate upstream to surrounding channel heads, where opposing signals between adjacent basins drive divide migration that modify available area for overland flow (e.g., Willett et al., 2014; O'Hara et al., 2019).

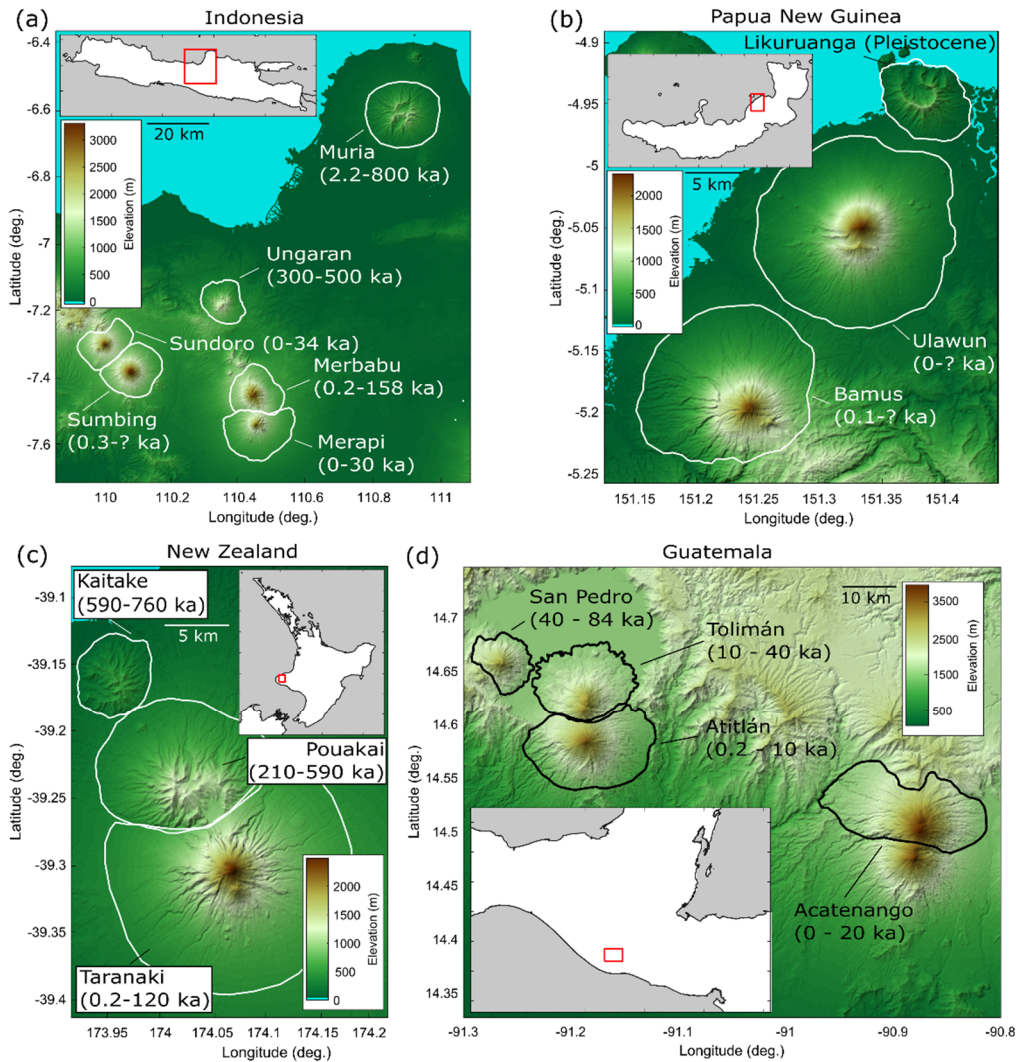
Work in the 20th century established foundational relationships between basin drainage areas, lengths, and slopes (e.g., Horton, 1945; Strahler, 1952; Hack, 1957; Flint, 1974), providing the basis for analyzing landscape disequilibrium and evolution in both tectonically-active (e.g., Kirby and Whipple, 2012; Fox et al., 2014) and passive (Prince and Spotila, 2013; Willett et al., 2014; Braun, 2018) regions. These relationships are built on the

42 assumption of a dominantly-dendritic fluvial network existing on a near-linear primary landform (e.g., a mountain
43 range; Castelltort and Simpson, 2006). Furthermore, basin competition is often considered in the simplified
44 configuration of a binary drainage system, where a divide supports only two opposing basins that compete across it
45 (e.g., Gilbert, 1909; Mudd and Furbish, 2007).

46 Although dendritic channel networks are most prevalent on Earth, they are not the only type of configuration.
47 Trellis, rectangular, parallel, and radial drainages also occur (Howard, 1967). The formation of these other drainages
48 often relate to the region's tectonic, volcanic, or glacial history, subsurface structure, or geometry of the primary
49 landform that they erode (Zernitz, 1932). However, compared to dendritic basins, studies that explore the geometries
50 and evolution of other drainage settings are scarce (e.g., Mejía and Niemann, 2008; Becerril et al., 2021; Hamawi et
51 al., 2022).

52 Volcanic edifices are characterized by radial drainages. In these settings, quantifying drainage evolution can be
53 challenging as these landforms experience interspersed, short-term eruptive episodes superimposed onto the long-
54 term degradation record (e.g., Thouret et al., 2014). These stochastic volcanic events often produce spatially-varying
55 excess sediment supply in the form of pyroclasts with varying grain properties that significantly alter fluvial
56 transport on decadal scales (e.g., Major et al., 2018; Hayes et al., 2002). Additionally, drainage formation can lag
57 behind surfacing by volcanic deposits over 1 – 100 kyr timescales due to transmission losses associated with
58 permeable volcanic material (e.g., lava flows, pyroclasts; Lohse and Dietrich, 2005; Jefferson et al., 2010; Sweeney
59 and Roering, 2017). Finally, the more symmetric drainage divide configuration typical of linear mountain ranges
60 breaks down on volcanic edifices due to their radial nature, with multiple catchments constrained to the conical
61 structure of the volcano and converging towards one or a few main summits. Despite these challenges, volcanic
62 edifices represent ideal primary landforms to investigate drainage evolution due to their well-defined conical initial
63 conditions, datable surfaces, and scarce inheritance from regional tectonics. Furthermore, quantifying the
64 relationships between edifice construction and drainage basin morphology provides new insight for investigating
65 edifices remotely, and can thus expand our understanding of basin dynamics while also complementing field-based
66 surveys to resolve volcano edifice histories.

67 Here, we explore the development of drainage basins and topography on stratovolcanoes from Indonesia, Papua
68 New Guinea, New Zealand, and Guatemala (Fig. 1). Using common hydrographic metrics and broad volcanic
69 histories, we determine stages of maturation during basin evolution and derive a new generalized model for
70 stratovolcano degradation that builds off of previous studies (Ollier, 1988). We then quantify divide mobility on
71 radial structures within the context of our conceptual model and discuss the applicability of our analyses to
72 characterize an edifice's history.



73

74 **Figure 1** – Regional maps of 16 analyzed edifices from (a) Indonesia, (b) Papua New Guinea, (c) New Zealand, and (d)
 75 Guatemala. Solid white lines in a-c and solid black lines in d represent edifice boundaries (boundary definition described in
 76 Methods). Text describes volcano names and known ages of activity (Table T2).

77 **2.0 Methods**

78 To constrain the temporal evolution of stratovolcano morphologies, we focus on closely-spaced volcano sets (Fig.
 79 1). The advantages of this approach are that within each respective region, 1) volcanoes were likely fed by similar
 80 magma sources (e.g., Locke and Cassidy, 1997; Haapala et al., 2005; Mulyaningsih and Shaban, 2020), constructed
 81 by similar volcanic deposits, and thus had similar volcanic shapes, 2) edifices experienced similar climate
 82 conditions, 3) volcano sets have radiometric ages related to their initiation and most recent eruption that are
 83 comparable, providing constraints on their overall lifespan, and 4) volcanoes within the same set were active over
 84 different time intervals, thus showing contrasting time-dependent degrees of dismantling within a short (10's of km)
 85 distance. In order to consider drainage basin evolution through fluvial erosion from the perspective of radial
 86 landforms, we exclude volcano massifs from our analysis, as well as any volcano with recognizable collapse scars,
 87 and only consider volcanoes that do not have an extensive glacial history. All analyzed volcanoes are classified as
 88 stratovolcanoes by the Smithsonian Global Volcanism Program (Global Volcanism Program, 2013).

89 **2.1 Edifice Delineation**

90 Although automated algorithms exist to generate volcano edifice boundaries (e.g., Bohnenstiehl et al., 2012;
91 Euillades et al., 2013), these often create conservative limits around the edifice that ignore lower flanks and volcano-
92 sedimentary aprons (e.g., O’Hara et al., 2020). We thus follow the method suggested by van Wees et al. (2021) to
93 delineate edifice boundaries from surrounding topography. Using 30-m Shuttle Radar Topography Mission (SRTM)
94 Digital Elevation Models (DEMs) (Farr et al., 2007), we first generate hillshade, aspect, and local slope rasters of
95 the raw topography. Lower edifice flanks are generally characterized by slope angles greater than some threshold
96 value (Karátson et al., 2012); we therefore remove short-wavelength variations of the slope raster by filtering it over
97 a 300 m wavelength (O’Hara et al., 2020) and contour regions that surpass a 3° slope threshold (van Wees et al.,
98 2021). Using these maps as visual aids, we then hand-draw boundaries that separate the edifice from surrounding
99 terrain. Afterwards, the DEMs are clipped using these boundaries to isolate the edifices for morphometric analysis.
100 The planform areas of edifice boundaries derived using this method range from 30.2 km² (Kaitake, New Zealand) to
101 432.7 km² (Muria, Indonesia).

102 **2.2 Edifice Basin Morphology**

103 We analyze edifice basin morphologies with DrainageVolc, a series of scripts modified from TopoToolbox
104 (Schwanghart and Scherler, 2014), which is designed to investigate volcanic topography through a set of
105 topography-, drainage-, and channel-based analyses. The metrics considered here are commonly used within
106 tectonic settings but have not previously been applied to radial drainages. Figure 2 displays an example of our
107 methods using Ungaran volcano in Indonesia.

108 We first fill sinks in the DEM through TopoToolbox’s preprocessing algorithm (Schwanghart and Scherler, 2014) to
109 ensure continuous flow to the edifice boundary and extract drainage basins from topography using steepest-descent
110 flow routing (Fig. 2a). We then perform a series of analyses related to basin geometry. The lengths (L) of all basins
111 draining to the edifice boundaries are calculated by determining mid-point paths between basin divides
112 perpendicular to the Euclidean distance between the highest and lowest reaches of the basin, irrespective of whether
113 there is an actual flow channel in this path (Fig. 2d). Assuming basins with total drainage areas (A) greater than
114 some threshold (A_T) support overland flow, we explore the correlation between the lengths and drainage areas of
115 these basins through a power-law regression to derive the Hack’s Law relationship (Fig. 2b) for the edifice as (Hack,
116 1957)

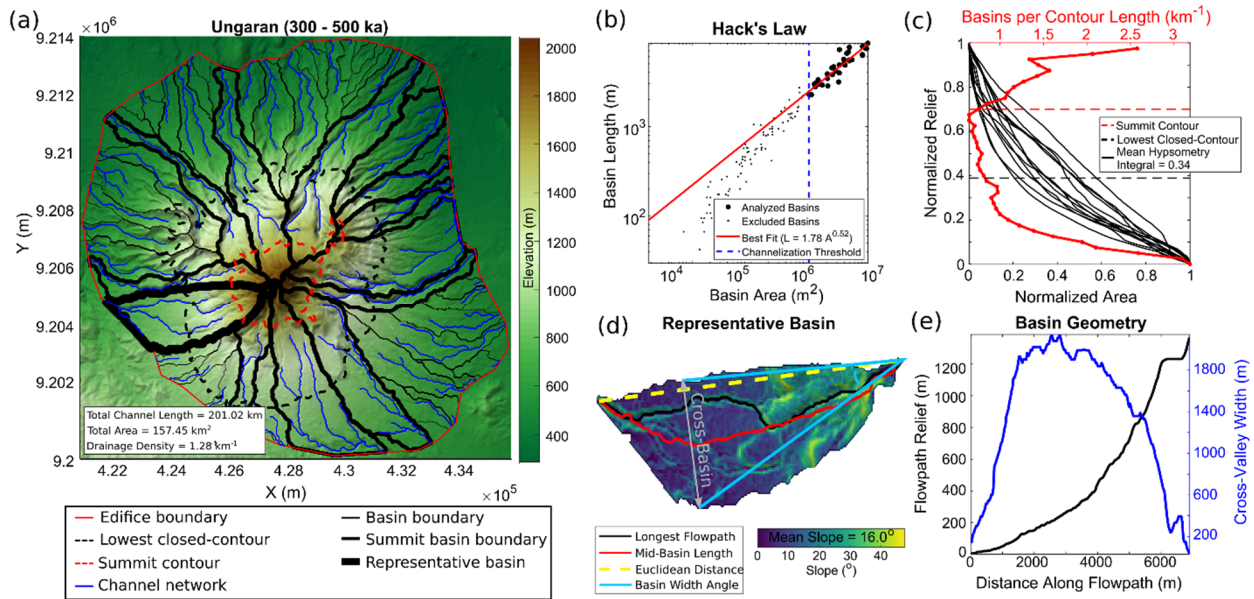
117
$$L = k_a A^H, \tag{1}$$

118 where k_a and H are Hack’s coefficient and exponent, respectively. H values are compared across edifices as this
119 exponent describes general basin geometry, with values of ~0.47 – 0.6 typically attributed to dendritic systems
120 (Hack, 1957; Mueller, 1972). Our Hack’s Law derivation uses basin lengths as opposed to typical flow path lengths
121 to remove the effects of channel sinuosity and focus explicitly on basin geometry; however, within the context of
122 our edifice basins, this derivation does not significantly alter our results, and values are thus comparable to those of
123 previous studies (Fig. S1). We also analyze the density of the edifice’s channel network by extracting flow paths

124 with drainage areas greater than A_T from the landform, and calculate the edifice-scale drainage density as (Horton,
 125 1945)

$$126 \quad DD = \frac{\sum L_c}{A_E}, \quad (2)$$

127 where $\sum L_c$ is the cumulative sum of all channel lengths and A_E is the planform area of the edifice's boundary (Fig.
 128 2a). Using an automated slope-area analysis of basins to determine the drainage area threshold that best corresponds
 129 with the power-law decrease in slope (Montgomery and Dietrich, 1994) for each edifice (Supplemental text; Fig.
 130 S2), we find A_T ranges between 0.32 – 1.62 km², with a mean threshold of 0.85 km² (Table T1). For consistency
 131 across all edifices, we assume a constant drainage area threshold of 1.0 km² to delineate networks. Sensitivity
 132 analysis (Fig. S3) demonstrates that although the selection of A_T does not significantly impact the general behavior
 133 of drainage density results, Hack's Law exponent is more sensitive to this choice.



134

135 **Figure 2** – Analyzed basin metrics. **a:** Example from the map of Ungaran volcano (Indonesia), colored lines defined in the
 136 legend. **b:** Hack's Law relationship between basin areas and lengths. Black circles are basins used in the power-law analysis,
 137 black dots are excluded basins; blue-dashed line is the drainage area threshold (A_T ; 1.0 km²) for channelization. **c:** Scaled edifice
 138 metrics. Red line shows normalized number of basins along elevation contours. Black lines are summit basin hypsometry curves.
 139 **d:** Local slope and geometry values of representative basin (thick black line in 2a). Gray double-arrow represents cross-basin
 140 direction (i.e., the extent of the basin) perpendicular to the Euclidean basin length. **e:** Cross-basin values along basin shown in 2d.
 141 Black line is relief along the flowpath, blue line is cross-valley width.

142 Afterwards, we calculate mean values of basin geometries on each edifice. Rather than analyze the geometry of all
 143 basins that exist on a volcano, we limit our analysis to larger basins that best characterize the edifice's drainage, and
 144 thus its dismantling. These large characteristic basins may be determined using a variety of methods, such as
 145 through an arbitrary number or percentage of basin sizes, using the basins that are within some radial distance of the
 146 edifice's peak, or determining basins that extend to some portion of the edifice's height. Determining characteristic
 147 basins by an arbitrary number or percentage of basin sizes may introduce bias as the population of basins drastically

148 varies between edifices (Fig. 8a), whereas determining characteristic basins by radial distance from the edifice's
 149 peak introduces geometric constraints as edifice shapes often deviate from the textbook symmetric, single-peaked
 150 edifice, instead developing large, irregular summit regions that are defined by high topography and multiple peaks
 151 (e.g., Karátson et al., 1999; Grosse et al., 2012). As slope (and thus elevation) is an essential component of erosion
 152 and basin development (Hack, 1957; Flint, 1974), we define characteristic basins as those that reach the edifice's
 153 summit region. However, we note that defining characteristic basins based on radial distance can produce different
 154 trends (Fig. S4) and may be more appropriate for some of our analyzed metrics (Section 5.3).

155 Generating a series of elevation contours along the edifice at intervals of 2.5% of the edifice's relief, we calculate
 156 the number of basins that intersect each contour, normalized by the contour's length (Fig. 2c, red line). For all
 157 edifices, we define the edifice's summit as the upper 30% of the edifice's relief, and thus consider the basins that
 158 reach this summit region (referred here as *summit basins*) as those that best characterize the edifice's drainage
 159 development. We then determine summit basin numbers, mean basin slopes (Fig. 2d), basin lengths (L_B ; Fig. 2d, red
 160 line), basin reliefs (Fig. 2e, black line), and maximum cross-basin widths (W_B ; Fig. 2e, blue line). To compare
 161 values across edifices of varying sizes, summit basin numbers are normalized by the length of the summit contour
 162 (Fig. 2c) and basin reliefs are normalized by the relief of the entire edifice. We also utilize the radial nature of
 163 edifices to generate normalized values of basin length (L'_B) and width (W'_B) as

$$164 \quad L'_B = \frac{L_B}{L_E}, \quad (3)$$

165 and

$$166 \quad W'_B = 2 \tan^{-1} \left(\frac{W_B/2}{L_{WB}} \right), \quad (4)$$

167 respectively, where L_E is the edifice's effective radius, defined as the radius of the circle with the same planform
 168 area (A_E) as the edifice's boundary ($L_E = \sqrt{A_E / \pi}$), and L_{WB} is the distance from the highest point within a basin to
 169 where the basin is widest. W'_B thus converts basin widths into an angle relative to the summit (Fig. 2d, light blue
 170 lines). Mean values of these quantities are then calculated for each edifice.

171 We also calculate mean summit basin hypsometry integrals for each edifice (Strahler, 1952; Fig. 2c, black lines).
 172 Individual basin hypsometry curves (H_C) are derived by counting the number of basin pixels N_{PB} at or above
 173 normalized elevation values (\hat{Z} , ranging from 0 to 1); afterwards, these values are normalized by the total number of
 174 basin pixels ($N_{P_{Tot}}$) as

$$175 \quad H_C(\hat{Z}_I) = \frac{N_{PB}(\hat{Z} \geq \hat{Z}_I)}{N_{P_{Tot}}}, \quad (5)$$

176 where I is a counter over normalized elevation values from 0 to 1. Hypsometry integrals of each basin are calculated
 177 as the positive integration over the curves from eq. (5). These are also averaged for each edifice.

178 **2.3 Edifice Landform Morphology**

179 As well as studying the temporal evolution of drainages on edifices, we also consider the broad geometry of the
180 volcanoes. Grosse et al. (2009, 2012) developed the initial MorVolc algorithm in IDL, which quantifies edifice
181 morphologies through a series of size, shape, slope, orientation, peak, and summit parameters. Using the same
182 framework as DrainageVolc, we redeveloped the IDL code in Matlab, also utilizing the TopoToolbox DEM analysis
183 package (Schwanghart and Scherler, 2014). Both DrainageVolc and the updated MorVolc scripts are available for
184 use on GitHub (https://github.com/danjohara/Volc_Packages).

185 We analyze simple edifice geometry measurements with this updated version of MorVolc, including effective
186 radius, height, height-radius ratio, and mean slope of the main flank (edifice region between the lowest closed-
187 contour that encompasses the edifice and the summit contour, Fig. 2a). We also quantify the mean contour ellipticity
188 and irregularity indices of the main flank from the previously-computed contours. The ellipticity index (EI)
189 describes the elliptical nature of the edifice elevation contours, and is defined as

$$190 \quad EI = \frac{\pi(L_M/2)^2}{A_C}, \quad (6)$$

191 where L_M is the length of the major axis of a best-fitting ellipse through the contour and A_C is the area enclosed by
192 the contour (Grosse et al., 2012). The irregularity index (II) describes divergence of the contour from a smooth
193 ellipse as

$$194 \quad II = di_{contour}(di_{ellipse} - 1), \quad (7)$$

195 where di is the dissection index, defined as

$$196 \quad di = \frac{P_C}{2A_C} \sqrt{A_C/\pi}, \quad (8)$$

197 with P_C and A_C being the perimeter and area of the contour, respectively (Grosse et al., 2012). Finally, we also
198 incorporate new measurements within MorVolc, including the slope variance of the entire edifice (standard
199 deviation of all slope values divided by the mean slope, similar to roughness), as well as a minimum eroded volume
200 estimate. Eroded volume is estimated from a convex-hull reconstruction of the edifice, using the methodology
201 described in O'Hara and Karlstrom (2023), in which the footprints of individual elevation contours along the edifice
202 are altered to remove concave regions (assuming they represent incised topography), thus creating convex polygons.
203 Polygons are then interpolated in three dimensions to create a simplified, reconstructed edifice. Afterwards, the
204 current topography is subtracted from the reconstructed edifice and positive values (i.e., areas having been eroded)
205 are integrated to estimate the volume of eroded material. Finally, eroded volume is normalized as a percent relative
206 to the total reconstructed volume.

207 **2.4 Edifice Ages**

208 To explore morphological evolution through time, we correlate edifice landform and drainage basin metrics to
209 volcano ages of activity. We thus compile known eruption records of each volcano, with ages ranging from present
210 to early Pleistocene (Table T2). Volcanoes often have complex surface evolutions, with lifespans of activity that

211 range 100-1000 kyrs and characterized by episodes of stochastic growth interspersed with periods of erosion during
212 quiescence (e.g., Karátson et al., 1999; Lahitte et al., 2012). Furthermore, episodes of activity are often constrained
213 to localized regions of the edifice and thus do not fully resurface the entire landform (e.g., Civico et al., 2022).
214 Similarly, erosion across the edifice is typically non-uniform as local conditions are dependent on the age and type
215 of activity, as well as microclimates (e.g., Ferrier et al., 2013; Pierson and Major, 2014; Thouret et al., 2014; Ricci et
216 al., 2015).

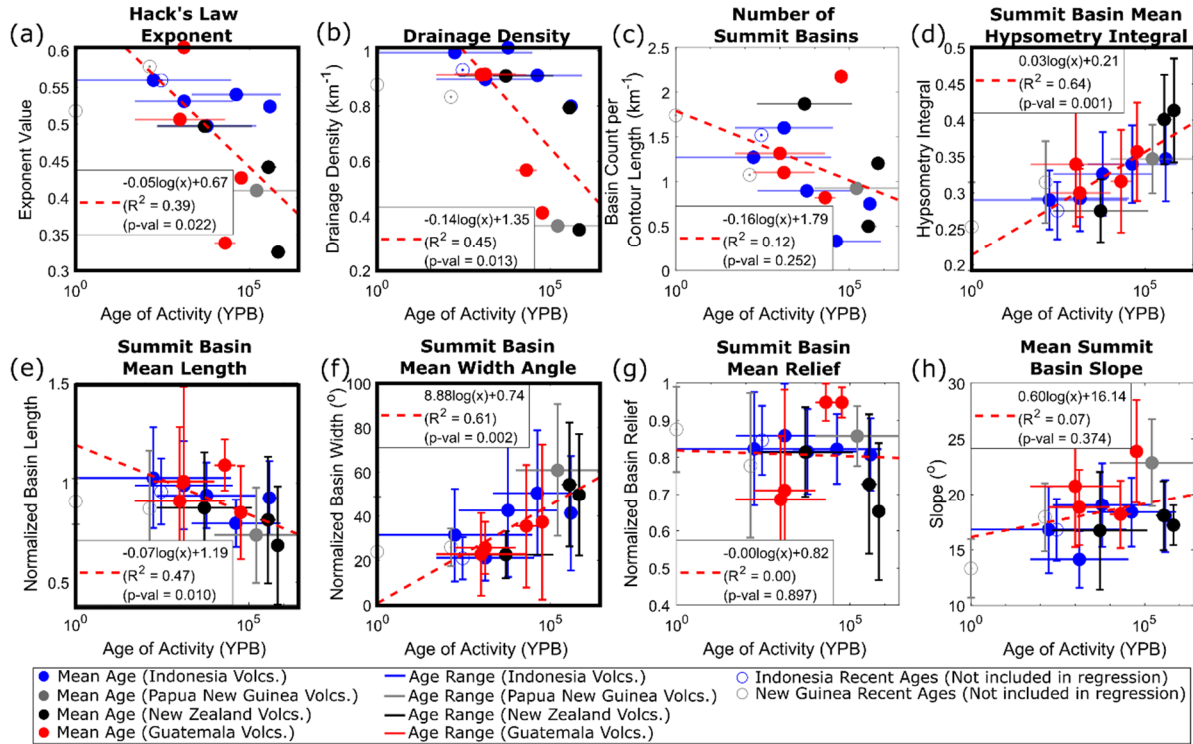
217 Despite the spatial and temporal heterogeneities of activity and erosion, we argue that a generalized morphologic
218 age of an edifice may be derived that quantifies the erosional state of the landform and relates to the edifice's
219 lithologic age. To account for the time differences between short-term events and the cumulative long-term history
220 on morphology, we define an edifice's age as a single value using the log-mean between the most recent eruption
221 and oldest date of activity. This definition thus accounts for the span of temporal magnitudes; however, we note that
222 using linear-mean ages produce similar results (Fig. S5) and recognize that other definitions of an edifice's
223 morphologic age are plausible (e.g., the time since the last eruption; Fig. S6). Afterwards, we analyze the temporal
224 evolution of edifice morphologies by fitting logarithmic relationships between edifice age and morphometric
225 parameters. Some volcanoes (Sumbing, Bamus, and Ulawun) have poorly-documented histories (only the most
226 recent eruption has been dated) and are therefore excluded from the regression. Conversely, Likuruanga is known to
227 have erupted only during the Pleistocene and is incorporated in the analysis.

228 **3.0 Results**

229 We find trends between stratovolcano age and our morphometry metrics through time (Figs. 3-4; Supplemental
230 Table T3). Considering all metrics, we find that edifice height, mean ellipticity index, normalized eroded volume,
231 Hack's Law exponent, drainage density, mean summit basin hypsometry integral, normalized basin length, and
232 normalized basin width have R^2 values ranging 0.39 – 0.77 and correlation p-values ≤ 0.05 . This list expands to
233 include effective edifice radius and mean irregularity index by removing a notable outlier (Muria, Indonesia; Fig. 4b,
234 4e), suggesting all of these metrics provide quantitative measures to characterize the overall maturity of the edifice.
235 Other metrics have weaker correlation values (0 – 0.25) and are statistically insignificant (p-values > 0.1), and thus
236 may be more sensitive to the initial edifice geometry or other processes that alter edifice morphology, or that age is
237 not a significant factor for these metrics. Muria (the noted outlier for effective edifice radius and irregularity index),
238 has an extensive volcanic history (from ~ 800 ka to 2 ka; McBirney et al., 2003; Global Volcanism Program, 2013)
239 and a morphology characterized by two broad fluvial networks on opposite flanks that are deeply incised into the
240 landform and may be associated with breached craters or flank collapses (Fig. 1a), suggesting this edifice may not fit
241 into the simple, radial volcano expectation of our dataset. We also note that due to the geometries that Acatenango
242 and Atitlán share with their sister volcanoes (Fuego and Tolimán, respectively; Fig. 1d), and our imposed definition
243 of an edifice's main flank (region between the lowest closed-contour and upper 30% of the edifice's height),
244 irregularity and ellipticity values could not be derived for these volcanoes.

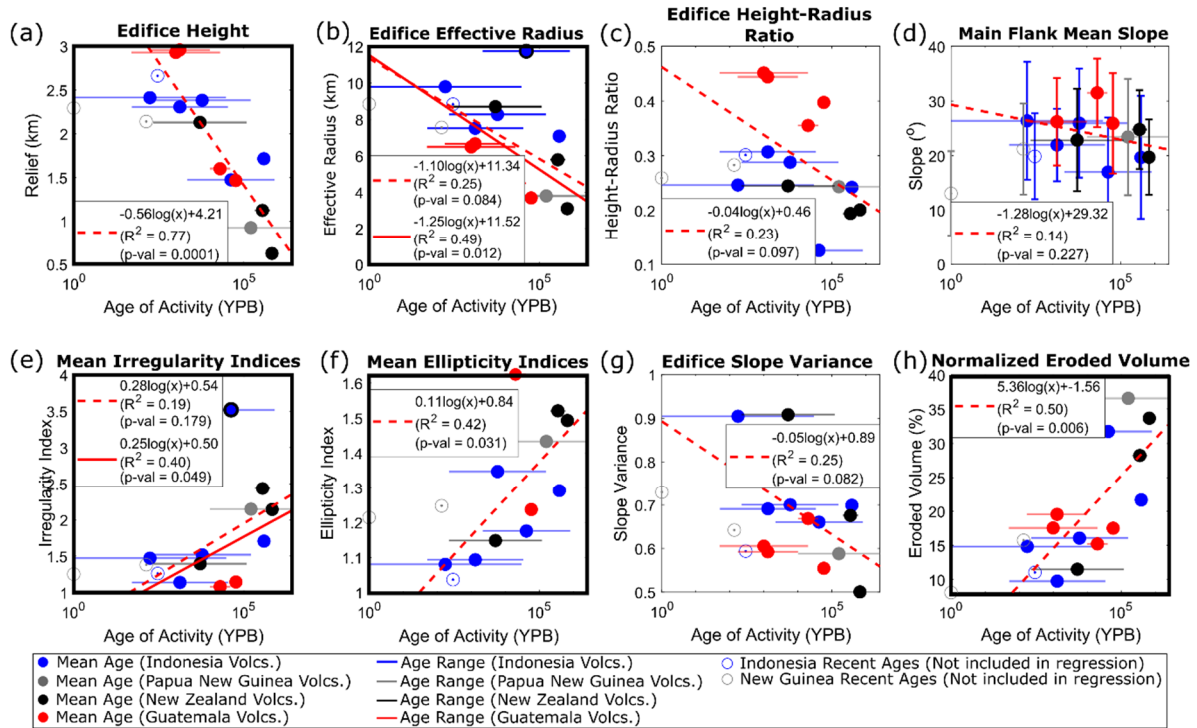
245 Of the statistically-significant metrics related to edifice drainage morphology, mean summit basin hypsometry
246 integral and normalized width increase through time, whereas Hack's Law exponent, drainage density, and mean

247 summit basin normalized length decrease (Fig. 3). Similarly, considering statistically-significant metrics related to
 248 the edifice as a primary landform, mean irregularity index, mean ellipticity index, and convex-hull based eroded
 249 volumes increase with age, while edifice height and effective radius decrease with age (Fig. 4).



250

251 **Figure 3** – Temporal relationships of drainage basin morphology metrics. Colors correspond to volcanic region. Horizontal lines
 252 are edifice age ranges of activity, with filled circles representing log-mean age. Vertical lines represent one standard deviations of
 253 values (where appropriate). Red-dashed lines and equations characterize logarithmic regressions; open circles are excluded from
 254 the regression due to age constraints. Thick black border highlights relationships with $R^2 > 0.35$.



255

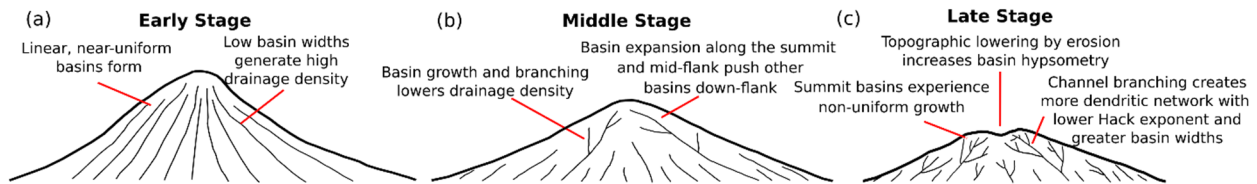
256 **Figure 4** – Temporal relationships of landform morphology metrics. Colors and symbols are same as those described in Fig. 3.
 257 Solid red lines in (b) and (e) are secondary regressions with outlier (Muria) excluded. Thick black border highlights relationships
 258 with $R^2 > 0.35$.

259 **4.0 Discussion**

260 **4.1 Generalized model for edifice degradation**

261 The evolution of stratovolcanoes as primary landforms and the drainage basins that erode them are inextricably
 262 linked. Our results thus establish a new framework for evaluating volcanic edifices by considering both the landform
 263 and its drainage systems. This evolutionary model expands on stages previously defined qualitatively (Ollier, 1988)
 264 and follows similar drainage evolution observed in badlands (Schumm, 1956).

265 Erosion of a stratovolcano can be described within the context of our metrics by considering a simplified, conical
 266 edifice (Fig. 5). In the initial stages of erosion (Fig. 5a, equivalent to ~10% normalized eroded volume in Fig. 4h),
 267 narrow (~20° normalized width angle) and uniform (normalized mean length near 1) drainages form that extend
 268 from the summit region to the lower flanks (i.e., ‘parasol ribbing’; Ollier, 1988), giving a high drainage density (~1
 269 km^{-1}) and Hack’s Law exponent (~0.6).



270

271 **Figure 5** – Conceptual model of edifice dissection based on analysis results. Thin black lines represent drainage systems.

272

273 As the edifice degrades to 30-40% normalized eroded volume (Fig. 4h) on 10-100 kyr timescales (Fig. 5b-c), both
274 its height and area decrease; however, height decreases faster, leading to a decrease in height-radius ratios. The
275 erosion of the edifice is accompanied by drainage basin growth, with summit basins expanding azimuthally along
276 the edifice to normalized basin widths of 40-60°, pushing the headwaters of other basins down the edifice flanks.
277 Furthermore, as summit basins expand, they incise into the edifice flanks and develop a more dendritic structure
278 associated with lower drainage density ($\sim 0.5 \text{ km}^{-1}$) and Hack's Law exponent (~ 0.4). This is accompanied by non-
279 uniform summit basin growth that causes normalized basin lengths to decrease below 1.

280 As the edifice erodes, processes occur over varying scales to alter general edifice morphology: 1) over the entire
281 edifice, erosion-driven topographic lowering occurs faster than horizontal areal loss of the edifice, creating a flatter
282 landform; and 2) at the scale of a basin, incision carves into the initially-planar flanks of the edifice, steepening
283 surrounding valley walls and increasing contour irregularity. The relationship between basin-scale incision and
284 edifice-scale flattening is recorded through summit basin hypsometry integrals, with increasing values suggesting
285 that edifice-scale flattening is the dominant process. This leads to a scale-dependent behavior in edifice morphology
286 – although the edifice as a landform is becoming flatter, incision causes topography to steepen locally. Previous
287 studies (e.g., Karátson et al., 2012; Dibacto et al., 2020; Ollier, 1988) suggest this simultaneous behavior causes the
288 edifice to lose its conical, single-peaked nature over longer ($> 1 \text{ Myr}$) timescales, developing high-relief drainage
289 divides over an extended summit region that support binary basin competition as the edifice erodes to the same relief
290 as surrounding terrain. Furthermore, we note that the decrease in edifice area through time differs from the
291 expectation of a sedimentary apron around the edifice that increases in area as the edifice erodes. Since edifice
292 boundaries are consistently defined in-part by a 3° topographic slope threshold, this suggests that on the 100 kyr
293 scale, sediment is not depositing at the edifice's base, but is being evacuated from the vicinity of the edifice, likely
294 through fluvial transport. The loss of sedimentary apron and overall decrease in edifice planform area was also
295 suggested by Ollier (1988) as an edifice transitions from its 'intact' stage to 'planèzes' stage.

296 This conceptual model represents a generalized view of edifice degradation, as a variety of processes (both volcanic
297 and erosional) can impact an edifice's morphology throughout its lifespan. Furthermore, other climate conditions not
298 considered here (e.g., glaciers, arid environments) are expected to alter the patterns and rates of basin evolution.
299 Nonetheless, we propose that, barring major events that significantly alter topography, stratovolcano degradation by
300 fluvial processes generally follows the model presented here.

301 **4.2 How do basins compete on radial structures?**

302 Our results suggest that drainages on radial structures are highly dynamic. From initially-uniform basin geometries,
303 preferential erosion causes basins near the summit to become more dominant and expand, forcing other basins
304 down-flank and generating a 'topographic hierarchy', with higher-order basins spanning the entire flank of the
305 edifice and lower-order basins occurring on lower sections, analogous to inferred basin evolution on linear fault
306 blocks (Talling et al., 1997). This hierarchy of basin ordering is a direct product of non-uniform basin development
307 over the edifice that contributes to the preservation of less-eroded portions of the lower flanks (i.e., planèzes; Ollier,
308 1988).

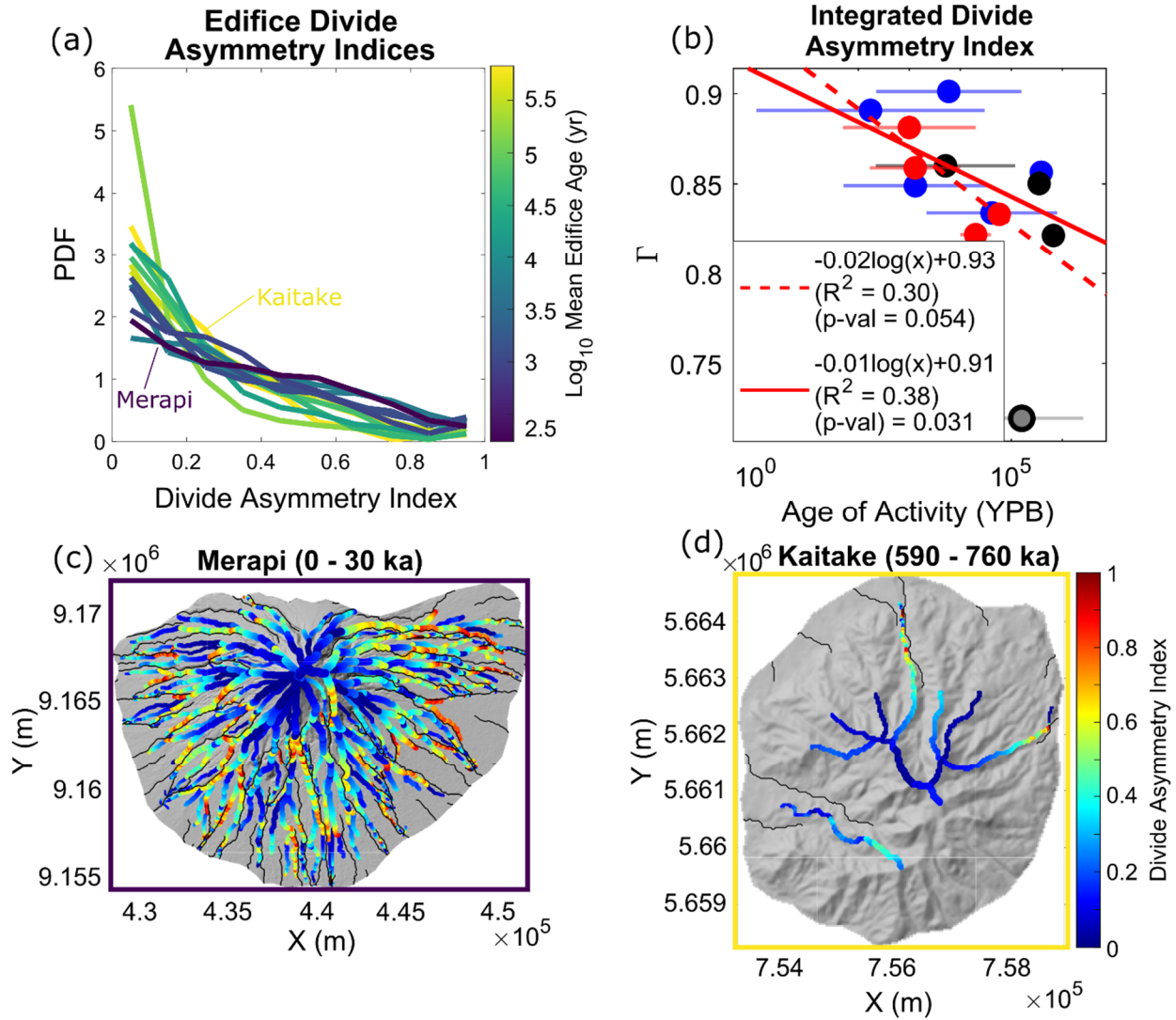
309 Non-uniform basin development and transience is a natural component of landscape evolution (e.g., Hasbargen and
310 Paola, 2000); however, various factors (both volcanic and non-volcanic) can influence erosional patterns and
311 accentuate basin growth across volcanic edifices. These may include 1) local slope changes associated with
312 magmatic intrusions (e.g., Wicks et al., 2002; Biggs et al., 2010; Castro et al., 2016) or mass-wasting (e.g., Ui and
313 Glicken, 1986; Shea and van Wyk de Vries, 2008); 2) variable volcanic eruption activity that increase sediment
314 loads (Hayes et al., 2002; Pierson and Major, 2014), alter infiltration and rock erodibility (e.g., Wells et al., 1985;
315 Sklar and Dietrich, 2001; Jefferson et al., 2010), or remove bedrock through scouring by pyroclasts (Gase et al.,
316 2017) or melting by lava flows (i.e., thermal erosion; Kerr, 2001) during deposition; 3) non-uniform changes in
317 overland flow and stream power associated with breached craters (e.g., Karátson et al., 1999) or edifice-scale
318 precipitation gradients (e.g., Ferrier et al., 2013); and 4) downstream alterations to drainage channels that migrate
319 upstream as a propagating incision wave (i.e., knickpoints; Kirby et al., 2003; Cook et al., 2013; Perron and Royden,
320 2013). The long-term compilation of such processes helps drive non-uniform erosion across the edifice, which in
321 turn encourages divide migrations and changes in basin size and geometry. More specifically, basins that exhibit
322 higher erosion rates would tend to expand at the expense of their neighboring basins and potentially become the
323 dominant basins, while lower erosion rates will cause other basins to shrink and their boundaries to migrate further
324 down the edifice's flank.

325 The morphology of drainage divides is sensitive to differences in erosion between neighboring basins and can thus
326 be used to characterize basin competition. We quantify basin geometry unsteadiness through an exploration of
327 divide stability using the *divide asymmetry index* (*DAI*; Forte and Whipple, 2018; Scherler and Schwanghart, 2020),
328 calculated as the positive difference in hillslope relief (vertical distance between the ridge and nearest channel)
329 across a divide and normalized by the sum of hillslope reliefs, ranging between 0 (symmetric) and 1 (asymmetric).
330 We limit our analysis to only consider divides that correspond to fluvial basins (i.e., have drainage areas > 1.0 km²
331 (Scherler and Schwanghart, 2020).

332 Divide mobility is expressed using probability density functions (PDFs) of *DAI* for all volcanoes (Fig. 6a). A clear
333 temporal trend emerges – older volcanoes have larger distributions clustered around lower (< 0.4) *DAI* that rapidly
334 decrease with increasing *DAI*; while younger volcanoes show monotonically-decreasing distributions, with fewer
335 normalized populations of low-*DAI* and greater normalized populations of high-*DAI* values compared to older
336 volcanoes. Integrating these PDFs into single values (referred to here as Γ ; Fig. 6b) shows a moderate correlation
337 with age ($R^2 = 0.38$) with the removal of Likuruanga (Papau New Guinea) as an outlier, which may be associated
338 with a breached crater (Fig. 1b).

339 Combined with basin morphology trends (Fig. 3), this suggests younger volcanoes have basins with more uniform
340 planform geometries and less-stable basin configurations. As the edifice erodes, basin planform geometries become
341 less uniform, but develop more stable configurations as evidenced by the greater symmetry of hillslope relief across
342 divides. The relationship between basin non-uniformity and stability can be observed spatially by comparing *DAI*
343 values between Merapi (youngest) and Kaitake (oldest) volcanoes (Fig. 6c-d). Highest *DAI* values on both
344 volcanoes generally occur at the mid- and lower-flanks of the volcano, suggesting basin expansion occurs mainly

345 azimuthally along edifice flanks, rather than across the edifice summit. This spatial analysis highlights the process
 346 that generates topographic hierarchy – by expanding azimuthally, basin growth drives less-dominant basins down-
 347 flank through a zipping process, creating drainages with tapered geometries along the lower flanks.



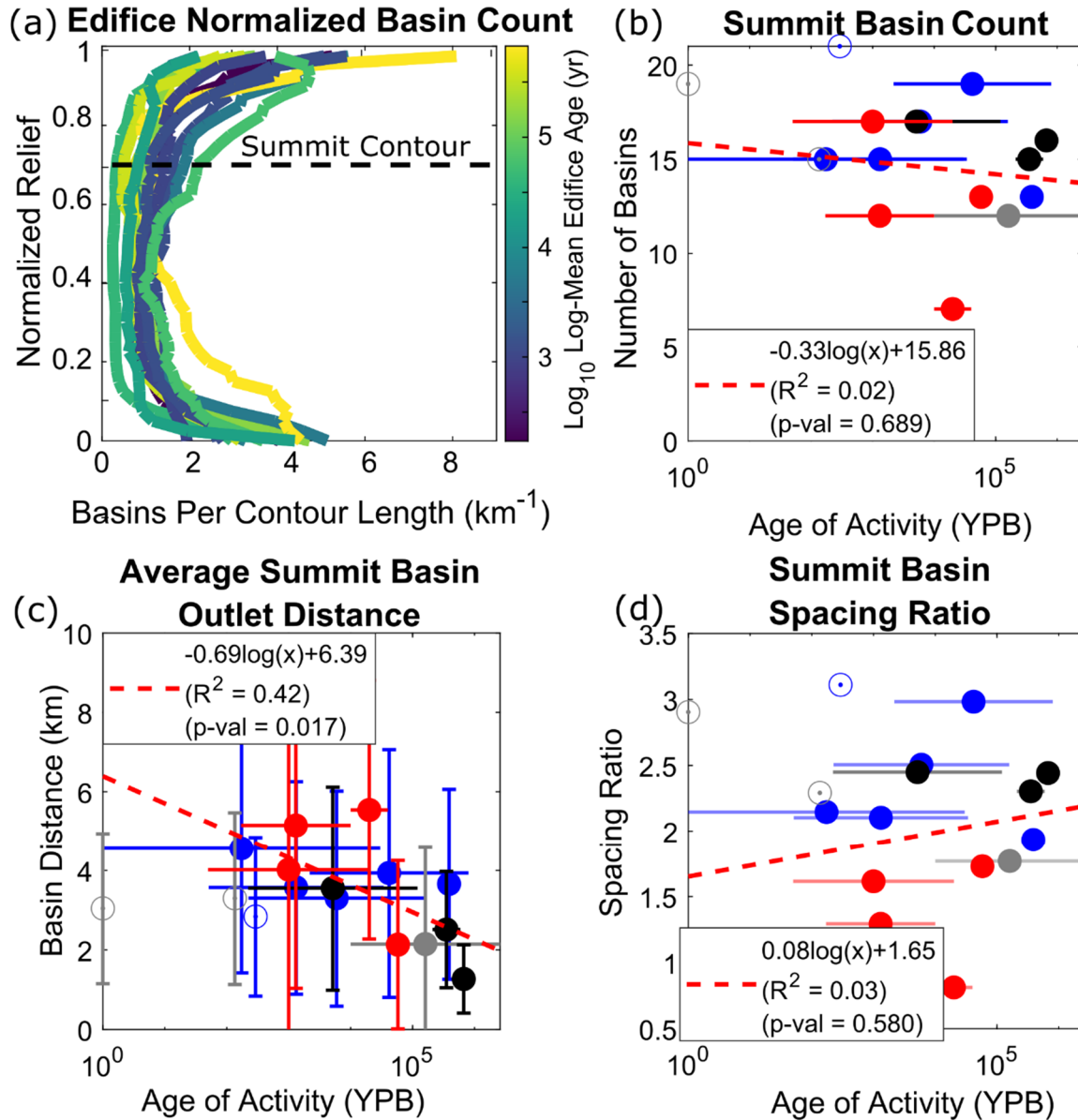
348

349 **Figure 6 – a:** Probability density functions (PDFs) of volcano divide asymmetry indices (*DAI*); colors correspond to log-mean
 350 edifice ages. **b:** Integral of PDFs (Γ) compared to edifice age. Colors and symbols are the same as Fig. 4. **c-d:** *DAI* values for (c)
 351 Merapi and (d) Kaitake at the divides, black lines are edifice channel network. Borders are colored with respect to Fig. 6a color
 352 scale.

353 4.3 Edifice basin widths and spacing

354 Our results show that edifices experience the same morphologic trends when considering the number of basins along
 355 edifice relief (Fig. 7a): lower flanks are characterized by normalized basin numbers between 2–5 km⁻¹, main flanks
 356 are characterized by relatively consistent normalized basin numbers < 2 km⁻¹, while the normalized basin numbers
 357 increase near the summit (upper 30% of the edifice). This trend appears to occur largely independent of age, even
 358 within the upper flank (as demonstrated by a low R^2 value of 0.12 at the summit contour, Fig. 3c), suggesting that
 359 this morphologic trend is a direct consequence of the conical nature of volcanoes. Furthermore, non-normalized

360 summit basin numbers also demonstrate a weak temporal trend, both at the upper 30% height designation (Fig. 7b)
 361 as well as other percentages (Fig. S7). This suggests that basins that initially form on the summit region may retain
 362 their topographic position as the edifice erodes. However, Fig. 3f demonstrates that these basins still widen through
 363 time, to a width angle of $\sim 60^\circ$, though further analysis on older volcanoes is needed to explore whether this persists
 364 on the Myr-timescale.



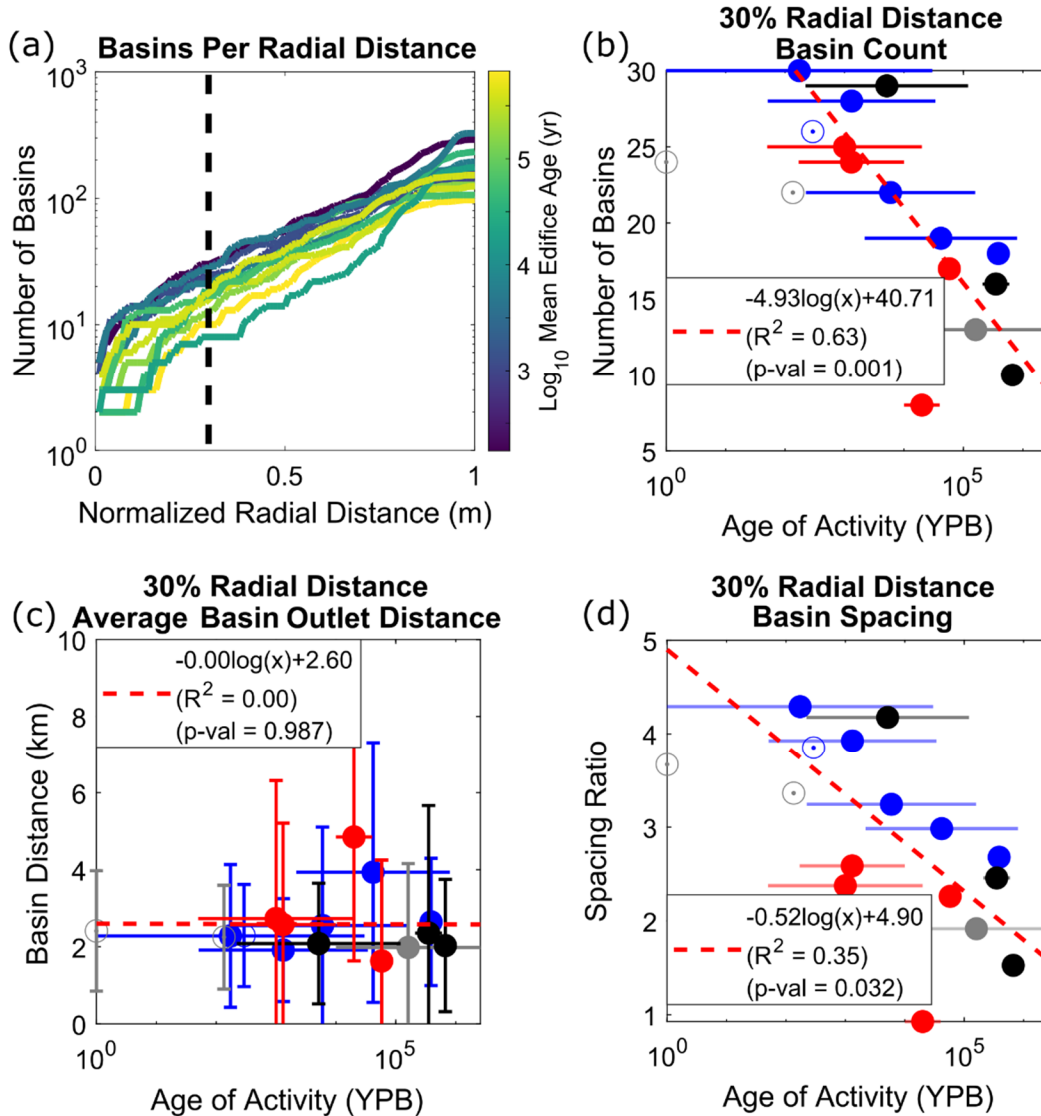
365 **Figure 7 – a:** Normalized number of basins along normalized relief for each volcano; colors are log-mean edifice age. **b:** Non-
 366 normalized number of summit basins (defined by the upper 30% of the edifice’s height; black-dashed line of a) compared to log-
 367 mean edifice age. **c:** Average along-perimeter summit basin distance compared to edifice age. **d:** Summit basin spacing ratio
 368 (data from Fig. 4b divided by data from c) compared to edifice age. Colors and symbols in b-d are the same as Fig. 3.
 369

370 An apparent contradiction occurs when comparing mean summit basin width angles to the number of summit basins.
 371 If all summit basins reached a width angle of $\sim 60^\circ$, it would be expected that only ~ 6 basins would exist at the

372 summit; however, Fig. 7b shows that the number of basins that reach the summit on most edifices is greater than 10.
373 This difference is a consequence of radial drainage basins achieving their maximum widths at different heights
374 relative to the height of the edifice, such that basin widths are normalized by different distances from the summit.
375 Indeed, as discussed in Section 4.2, divide asymmetry is most frequent in the mid- and lower-flanks of the edifice
376 (Fig. 6), thus accommodating largest basin widths at different sections of the flank.

377 If the number of basins that reach the summit is time invariant, how does this translate to the circumferential spacing
378 of their outlets at the base of the edifice? Hovius (1996) compiled the ratio between mountain belt half-widths
379 (distance between the major divide and mountain front, W_M) and distances between major drainage basin outlets
380 (those that reach the major divide; s) in 11 mountain ranges globally, and determined a globally-averaged spacing
381 ratio (W_M / s) of ~ 2 -3. We perform a similar analysis by dividing edifice effective radii by the average along-
382 perimeter spacing between summit basin outlets. Figs 4b and 7c show that while edifice effective radii decrease
383 through time, so does the average perimeter distance between summit basin outlets. These behaviors thus combine
384 to produce summit basin spacing ratios of $\sim 1 - 3$ (Fig. 7d), consistent with Hovius (1996) as well as modeling
385 studies of drainage patterns (Habousha et al., 2023). This suggests that while summit basins azimuthally expand
386 their widths, the edifice is also decreasing in area as the landform erodes, thus decreasing the distances between
387 summit basin outlets.

388 However, a different behavior emerges when considering basins by their radial distance relative to the edifice's peak
389 (Fig. 8), which is more sensitive to the areal expansion of basins along the edifice's flank. Plotting the non-
390 normalized number of basins as a function of radial distance (normalized by maximum radius for each edifice) and
391 time shows a clear temporal trend (Fig. 8a), with younger edifices having more basins along all sections of the
392 volcano (as schematized in Fig. 5). This trend becomes more apparent through the logarithmic regression between
393 edifice age and the number of basins that exist at 30% radial distance from the peak (Fig. 8b), with other normalized
394 distances showing the same behavior (Fig. S8). Conducting a similar outlet perimeter-distance analysis on these
395 basins shows that the average distance between basin outlets is relatively constant at ~ 2 km (Fig. 8c), giving a
396 temporal decrease in basin spacing ratios ($R^2 = 0.35$, Fig. 8d). This relationship suggests a dynamic in radial
397 drainage evolution related to landform geometry. Combined with other metrics, our results suggest that as the
398 edifice erodes and loses planform area through time, very small basins on the edifice's lower flanks likely become
399 erased while more dominant basins widen on the mid flank, thus causing basins that exist within 30% radial distance
400 of the edifice's summit to retain an approximately constant outlet distance along the shrinking perimeter.



401
 402 **Figure 8 – a:** Non-normalized number of basins as a function of normalized distance from the edifice’s peak; colors are log-
 403 mean edifice age, black-dashed line represents 30% normalized radial distance from the edifice’s peak (basins used for plots in
 404 b-d). **b:** Non-normalized number of basins compared to log-mean edifice age. **c:** Average along-perimeter basin distance
 405 compared to edifice age. **d:** Basin spacing ratio (data from Fig. 4b divided by data from c) compared to edifice age. Colors and
 406 symbols in b-d are the same as Fig. 3.

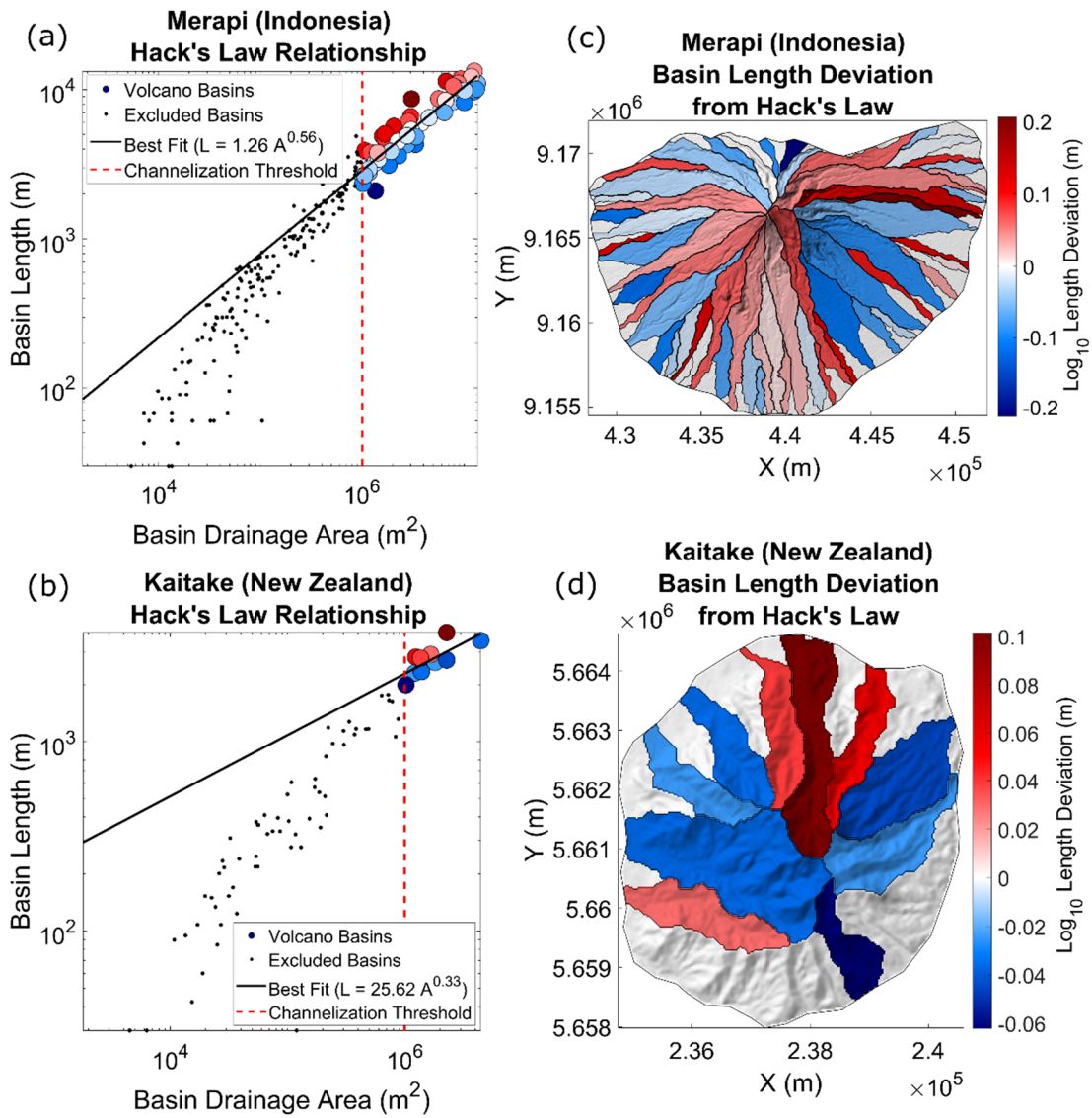
407 **4.4 Radial drainage basin area-length relationship**

408 As a final observation for volcanic edifice drainage basins, we consider basin geometries in reference to Hack’s
 409 power-law relationships between basin areas and lengths (Hack, 1957). Analyzing Hack’s Law regressions for
 410 Merapi and Kaitake (Fig. 9), the relationships between spatial location and basin geometries become apparent. On
 411 Merapi, basins less than 10^5 m^2 do not conform to the same power-law trend as those greater than 10^5 m^2 , whereas
 412 on Kaitake this break occurs at 10^6 m^2 . These smaller basins are constrained to the lowest regions of the edifices’
 413 flanks and likely correspond to non-channeled surfaces. Of those considered for the Hack’s Law regression, the
 414 log_{10} basin length deviation (D_L) from the power-law is calculated as

415 $D_L = \log_{10}(L_H(A)) - \log_{10}(L),$ (9)

416 where L_H is the basin length of the Hack's Law regression from a given basin's area (A), and L is the basin's length.
417 As expected from the geometric relationship, basins that fall below the power-law regression ($D_L < 0$) are wider,
418 and those that are above the power-law regression ($D_L > 0$) are narrower.

419 Calculating D_L for basins with areas greater than our imposed channelization threshold (1.0 km^2), one clear
420 observation is the presence of highly-elongated basins on Merapi that exist on the mid- to upper-flanks and have D_L
421 values > 0.15 (Fig. 9c). These basins appear wedged or pinched between larger basins and would be expected to not
422 have as much growth potential compared to their wider neighbors. Elongated basins also exist on Kaitake; however,
423 they do not have as high of a deviation (maximum $D_L \approx 0.1$; Fig. 9d). This may be a product of the lower number of
424 basins that exist on Kaitake, the overall lower amount of drainage area that Kaitake basins occupy, or an evolution
425 of basins towards more consistent patterns, thus decreasing the amount of variability from the power-law
426 relationship. On both Merapi and Kaitake, these elongated basins may further highlight the dynamics of basin
427 competition on radial structures – through drainage divide migration and areal loss (likely influenced by edifice-
428 scale sector collapses or regrowth events; Gertisser et al., 2023), less-erosive drainages become passive players to
429 more dominant basins and adopt non-standard geometries, becoming narrow, chute-like basins on the mid- and
430 upper-flanks.



431
 432 **Figure 9** – Hack’s Law analysis of (a, c) Merapi and (b, d) Kaitake. **a-b**: Basin drainage area – length relationships. Black lines
 433 represent Hack’s Law regressions. Colored circles correspond to the deviation from the regression trend (eq. 9), associated with
 434 the color bars in c and d. Red-dashed line is imposed 1.0 km² channelization threshold, black dots are basins less than the
 435 threshold and excluded from the regression. **c-d**: Maps showing the deviation of each basin from the best-fit power-law
 436 regression.

437 **4.5 How do radial drainages compare to other settings?**

438 Thus far, our discussion has focused on deriving a foundational understanding of how radial drainages on volcanic
 439 edifices evolve and compete. However, we note similarities between our interpretation and those from previous
 440 studies in other drainage settings. This leads to a simple question – is there a significant difference between radial
 441 and dendritic drainage development and evolution?

442 Our results show that basin formation on volcanic edifices follows the development of rills and gullies within
 443 badlands (Schumm, 1956). As radial drainages evolve and certain basins expand to become dominant features on the
 444 edifice, less-dominant basins become passive and are pushed down-flank, often adhering to non-standard geometries
 445 as imposed by their more-dominant neighbors (Habousha et al., 2023; Beeson and McCoy, 2022). The dynamics of

446 this basin competition and formation of passive basins are demonstrated by edifice basin spacing ratios. Summit
447 basins on edifices have spacing ratios that appear time-independent and fit within the range of values observed in
448 linear mountain ranges globally (Hovius, 1996) (Fig. 7), suggesting this ratio is set during the initial stages of basin
449 formation – an attribute of basin evolution that has been shown to occur on linear fault blocks (Talling et al., 1997;
450 Habousha et al., 2023). However, basins that are within a radial distance from the summit that is 30% of the
451 edifice’s maximum radius do experience a temporally-decreasing spacing ratio and constant distance between
452 outlets (Fig. 8), capturing the development of a basin topographic hierarchy along the edifice – a behavior not
453 previously observed. Finally, our drainage divide analysis on volcanic edifices suggest that radial drainage basins
454 evolve towards a stable basin configuration as topography matures towards a dynamic equilibrium, similar to
455 regional landscape evolution globally (e.g., Perron and Royden, 2013; Willett et al., 2014).

456 This comparison suggests that drainage development and evolution on radial structures are largely similar to those
457 occurring within linear mountain settings. However, some differences still occur, particularly in relation to basin
458 geometries imposed by the larger-scale, radial primary landform. Dendritic drainages in linear mountain belts and
459 fault blocks are characterized by their leaf-like geometries (e.g., Zernitz, 1932; Strahler, 1952; Talling et al., 1997),
460 having a broad headwater region that decreases towards the outlet to a tapered point. Although radial drainages also
461 have tapered outlets and basin widths increase upstream, these widths are hindered by the conical geometry of the
462 primary landform and convergence of multiple basins towards the summit, leading to a tapered headwater as well as
463 a tapered outlet. This geometric constraint is well-demonstrated by the drainages on Merapi (Fig. 9c), where summit
464 basins are generally widest on the lower- or mid-flanks; however, this trend is not as obvious on Kaitake (Fig. 9d),
465 where erosion has dissected the landform and weakened the conical influence of the edifice on basin geometries.
466 Furthermore, as edifice drainages are limited to a conical landform, their evolution and configuration are constrained
467 by a cumulative areal limit. As opposed to linear mountain ranges (where a morphologic change in one basin
468 impacts its neighbors, which then impacts their neighbors as a cascading chain across the landscape), on volcanic
469 edifices, a morphologic change in one basin (particularly a dominant basin) may directly impact the erosional state
470 and morphology of most other basins on the landform due to the high number of basins that may share a divide with
471 this basin. This areal effect on radial basin evolution may be further augmented by the higher diversity of underlying
472 host rocks between edifice basins associated with magmatic and volcanic products (e.g., tephra deposits, lava flows,
473 and intrusions) that is not as prevalent within linear mountain ranges.

474 Despite the differences in basin geometries and interactions discussed above, edifice-averaged morphometric values
475 (e.g., Hack’s Law exponent, drainage density, mean basin hypsometry, mean basin slopes) are similar to those of
476 other settings (Hack, 1957; Strahler, 1952; Horton, 1945). This suggests that although radial drainages experience
477 phenomena that differ from those typically experienced in dendritic settings, drainage development, geometries, and
478 competition largely follow those of dendritic patterns. As volcanic surfaces are easily datable and their ages can
479 often vary by orders magnitude on a single edifice, volcanoes thus represent ideal locations for studying terrain
480 evolution over varying temporal scales within a general framework.

481 **4.6 Basin morphology capturing volcanic processes**

482 In this study, we considered edifice morphologies using mean values over the entire edifice. However, our metrics
483 also allow for the comparison of basin morphologies on a single edifice. Variations associated with these metrics
484 would likely relate to spatially-localized attributes of aggradation, degradation, and climate, and would thus provide
485 a quantitative method to disentangle these signals using topography. For example, edifice flanks that have been
486 resurfaced by large volcanic deposits or destroyed by sector collapses should exhibit younger drainage networks
487 according to the metrics explored here, and are expected to differ from other parts of the volcano. Furthermore,
488 alterations to the erosional efficiency of a basin by tephra accumulation or lava flow emplacement should create
489 spatial variability that can be quantified by similar analyses. These concepts should be tested over well-constrained
490 cases and would be beneficial for both preliminary fieldwork and to approximate relative volcanic chronologies
491 remotely. Our model for edifice degradation, radial drainage evolution, and divide stability thus provides a first step
492 to deconvolving the various signals that relate to edifice morphology. This presents new avenues of exploration for
493 the volcanology community to interrogate volcanic histories from topography, and for the geomorphic community to
494 investigate surface evolution on landforms that often fall outside standard tectonic studies.

495 **5.0 Conclusion**

496 Volcanic edifices represent a class of primary landforms whose erosion remains relatively unexplored. We analyzed
497 the degradational histories of stratovolcanoes using a set of metrics that have not previously been considered for
498 radial drainage networks. We show that these metrics relate to the overall age of a volcano and propose a new
499 general model for the temporal evolution of edifice drainage morphology. Divide stability analysis underscores the
500 dynamic nature of basin evolution, and suggests that radial drainage networks initiate with nearly-uniform
501 geometries and unstable configurations that evolve towards non-uniform basin geometries and more stable
502 configurations to generate a basin topographic hierarchy on volcanoes. Finally, comparing basin geometries,
503 configurations, and outlet spacing between basins that exist on volcanic edifices to those that exist on linear
504 mountain ranges highlights similarities and differences between radial and dendritic drainage basins.

505 **6.0 Code availability**

506 DrainageVolc and MorVolc codes are available at https://github.com/danjohara/Volc_Packages.

507 **7.0 Data availability**

508 Collected edifice data is included in the supplement as both an Excel file and shapefile.

509 **8.0 Author contribution**

510 All authors provided editorial advice on the manuscript. DO'H wrote the DrainageVolc and updated MorVolc codes,
511 conducted the morphology analyses, and wrote the manuscript. RMJvW assisted in data collection, determined
512 edifice boundaries from topography, and tested DrainageVolc/MorVolc. LG and BC gave advice on drainage basin
513 morphology and evolution, while PG, PL, and GK provided insight on volcanic edifice morphology, evolution, and
514 general volcano ages. MK secured funds and coordinated the project, giving advice on the research direction,
515 analyses, and interpretation.

516 **9.0 Competing interests**

517 The authors declare that they have no conflict of interest.

518 **10.0 Acknowledgement**

519 This research was funded through the EVoLvE project, Junior FWO project grant G029820N of the Fonds
520 Wetenschappelijke Onderzoek – Vlaanderen.

521 **11.0 References**

522 Becerril, L., Lara, L. E., and Astudillo, V. I.: The strong competition between growth and erosive processes on the
523 Juan Fernández Archipelago (SE Pacific, Chile), *Geomorphology*, 373, 107513,
524 <https://doi.org/10.1016/j.geomorph.2020.107513>, 2021.

525 Beeson, H. W. and McCoy: Disequilibrium river networks dissecting the western slope of the Sierra Nevada,
526 California, USA, record significant late Cenozoic tilting and associated surface uplift, *Bull. Geol. Soc. Am.*, 134,
527 2809–2853, <https://doi.org/10.1130/B36517.1>, 2022.

528 Biggs, J., Mothes, P., Ruiz, M., Amelung, F., Dixon, T. H., Baker, S., and Hong, S. H.: Stratovolcano growth by co-
529 eruptive intrusion: The 2008 eruption of Tungurahua Ecuador, *Geophys. Res. Lett.*, 37,
530 <https://doi.org/10.1029/2010GL044942>, 2010.

531 Bishop, P.: Drainage rearrangement by river capture, beheading and diversion, *Prog. Phys. Geogr.*, 19, 449–473,
532 1995.

533 Bohnenstiehl, D. W. R., Howell, J. K., White, S. M., and Hey, R. N.: A modified basal outlining algorithm for
534 identifying topographic highs from gridded elevation data, Part 1: Motivation and methods, *Comput. Geosci.*, 49,
535 308–314, <https://doi.org/10.1016/j.cageo.2012.04.024>, 2012.

536 Braun, J.: A review of numerical modeling studies of passive margin escarpments leading to a new analytical
537 expression for the rate of escarpment migration velocity, *Gondwana Res.*, 53, 209–224,
538 <https://doi.org/10.1016/j.gr.2017.04.012>, 2018.

539 Castelltort, S. and Simpson, G.: River spacing and drainage network growth in widening mountain ranges, *Basin*
540 *Res.*, 18, 267–276, <https://doi.org/10.1111/j.1365-2117.2006.00293.x>, 2006.

541 Castelltort, S., Simpson, G., and Darriulat, A.: Slope-control on the aspect ratio of river basins, *Terra Nov.*, 21,
542 265–270, <https://doi.org/10.1111/j.1365-3121.2009.00880.x>, 2009.

543 Castelltort, S., Goren, L., Willett, S. D., Champagnac, J. D., Herman, F., and Braun, J.: River drainage patterns in
544 the New Zealand Alps primarily controlled by plate tectonic strain, *Nat. Geosci.*, 5, 744–748,
545 <https://doi.org/10.1038/ngeo1582>, 2012.

546 Castro, J. M., Cordonnier, B., Schipper, C. I., Tuffen, H., Baumann, T. S., and Feisel, Y.: Rapid laccolith intrusion
547 driven by explosive volcanic eruption, *Nat. Commun.*, 7, 1–7, <https://doi.org/10.1038/ncomms13585>, 2016.

548 Civico, R., Ricci, T., Scarlato, P., Taddeucci, J., Andronico, D., Del Bello, E., D’Auria, L., Hernández, P. A., and
549 Pérez, N. M.: High-resolution Digital Surface Model of the 2021 eruption deposit of Cumbre Vieja volcano, La
550 Palma, Spain, *Sci. Data*, 9, 1–7, <https://doi.org/10.1038/s41597-022-01551-8>, 2022.

551 Cook, K. L., Turowski, J. M., and Hovius, N.: A demonstration of the importance of bedload transport for fluvial
552 bedrock erosion and knickpoint propagation, *Earth Surf. Process. Landforms*, 38, 683–695,
553 <https://doi.org/10.1002/esp.3313>, 2013.

554 Dibacto, S., Lahitte, P., Karátson, D., Hencz, M., Szakács, A., Biró, T., Kovács, I., and Veres, D.: Growth and
555 erosion rates of the East Carpathians volcanoes constrained by numerical models: Tectonic and climatic
556 implications, *Geomorphology*, 368, 107352, <https://doi.org/10.1016/j.geomorph.2020.107352>, 2020.

557 Duvall, A. R. and Tucker, G. E.: Dynamic Ridges and Valleys in a Strike-Slip Environment, *J. Geophys. Res. F*
558 *Earth Surf.*, 120, 2016–2026, <https://doi.org/10.1002/2015JF003618>, 2015.

559 Euillades, L. D., Grosse, P., and Euillades, P. A.: NETVOLC: An algorithm for automatic delimitation of volcano
560 edifice boundaries using DEMs, *Comput. Geosci.*, 56, 151–160, <https://doi.org/10.1016/j.cageo.2013.03.011>, 2013.

561 Farr, T. G., Rosen, P. A., Caro, E., Crippen, R., Duren, R., Hensley, S., Kobrick, M., Paller, M., Rodriguez, E.,
562 Roth, L., Seal, D., Shaffer, S., Shimada, J., Umland, J., Werner, M., Oskin, M., Burbank, D., and Alsdorf, D.: The
563 Shuttle Radar Topography Mission, *Rev. Geophys.*, 45, 1–43, 2007.

564 Ferrier, K. L., Huppert, K. L., and Perron, J. T.: Climatic control of bedrock river incision, *Nature*, 496, 206–209,
565 <https://doi.org/10.1038/nature11982>, 2013.

566 Flint, J. J.: Stream gradient as a function of order, magnitude, and discharge, *Water Resour. Res.*, 10, 969–973,
567 <https://doi.org/10.1029/WR010i005p00969>, 1974.

568 Forte, A. M. and Whipple, K. X.: Criteria and tools for determining drainage divide stability, *Earth Planet. Sci. Lett.*,
569 493, 102–117, <https://doi.org/10.1016/j.epsl.2018.04.026>, 2018.

570 Fox, M., Goren, L., May, D. A., and Willett, S. D.: Inversion of fluvial channels for paleorock uplift rates in Taiwan,
571 *J. Geophys. Res. Earth Surf.*, 119, 1853–1875, <https://doi.org/10.1002/2014JF003196>, 2014.

572 Gase, A. C., Brand, B. D., and Bradford, J. H.: Evidence of erosional self-channelization of pyroclastic density
573 currents revealed by ground-penetrating radar imaging at Mount St. Helens, Washington (USA), *Geophys. Res.*
574 *Lett.*, 44, 2220–2228, <https://doi.org/10.1002/2016GL072178>, 2017.

575 Gertisser, R., Troll, V. R., Walter, T. R., Nandaka, I. G. M. A., and Ratdomopurbo, A.: Merapi Volcano: Geology,
576 Eruptive Activity, and Monitoring of a High-Risk Volcano, Springer Nature, 2023.

577 Gilbert, G. K.: The Convexity of Hilltops, *J. Geol.*, 17, 344–350, 1909.

578 Global Volcanism Program: Volcanoes of the World, v. 4.10.5 (27 Jan 2022), *Smithson. Inst.*, 2013.

579 Grosse, P., van Wyk de Vries, B., Petrinovic, I. A., Euillades, P. A., and Alvarado, G. E.: Morphometry and
580 evolution of arc volcanoes, *Geology*, 37, 651–654, <https://doi.org/10.1130/G25734A.1>, 2009.

581 Grosse, P., van Wyk de Vries, B., Euillades, P. A., Kervyn, M., and Petrinovic, I. A.: Systematic morphometric
582 characterization of volcanic edifices using digital elevation models, *Geomorphology*, 136, 114–131,
583 <https://doi.org/10.1016/j.geomorph.2011.06.001>, 2012.

584 Haapala, J. M., Escobar Wolf, R., Vallance, J. W., Rose, W. I., Griswold, J. P., Schiling, S. P., Ewert, J. W., and
585 Mota, M.: Volcanic Hazards at Atitlán Volcano, Guatemala, *Open-File Rep.*, 2005.

586 Habousha, K., Goren, L., Nativ, R., and Gruber, C.: Plan-Form Evolution of Drainage Basins in Response to
587 Tectonic Changes: Insights From Experimental and Numerical Landscapes, *J. Geophys. Res. Earth Surf.*, 128, 1–24,
588 <https://doi.org/10.1029/2022jf006876>, 2023.

589 Hack, J. T.: Studies of longitudinal stream profiles in Virginia and Maryland, *USGS Prof. Pap.* 249, 97, 1957.

590 Hamawi, M., Goren, L., Mushkin, A., and Levi, T.: Rectangular drainage pattern evolution controlled by pipe cave
591 collapse along clastic dikes, the Dead Sea Basin, Israel, *Earth Surf. Process. Landforms*, 47, 936–954,
592 <https://doi.org/10.1002/esp.5295>, 2022.

593 Han, J., Gasparini, N. M., and Johnson, J. P. L.: Measuring the imprint of orographic rainfall gradients on the
594 morphology of steady-state numerical fluvial landscapes, *Earth Surf. Process. Landforms*, 40, 1334–1350,
595 <https://doi.org/10.1002/esp.3723>, 2015.

596 Hasbargen, L. E. and Paola, C.: Landscape instability in an experimental drainage basin, *Geology*, 28, 1067–1070,
597 [https://doi.org/10.1130/0091-7613\(2000\)28<1067:LIIAED>2.0.CO;2](https://doi.org/10.1130/0091-7613(2000)28<1067:LIIAED>2.0.CO;2), 2000.

598 Hayes, S. K., Montgomery, D. R., and Newhall, C. G.: Fluvial sediment transport and deposition following the 1991
599 eruption of Mount Pinatubo, *Geomorphology*, 45, 211–224, [https://doi.org/10.1016/S0169-555X\(01\)00155-6](https://doi.org/10.1016/S0169-555X(01)00155-6), 2002.

600 Horton, R. E.: Erosional development of streams and their drainage basins; hydrological approach to quantitative
601 morphology, *Geol. Soc. Am. Bull.*, 56, 275–370, <https://doi.org/10.1130/0016->

602 7606(1945)56[275:EDOSAT]2.0.CO;2, 1945.

603 Hovius, N.: Regular spacing of drainage outlets from linear mountain belts, *Basin Res.*, 8, 29–44,
604 <https://doi.org/10.1111/j.1365-2117.1996.tb00113.x>, 1996.

605 Howard, A. D.: Drainage Analysis in Geologic Interpretation: A Summation, *Am. Assoc. Pet. Geol. Bull.*, 51,
606 <https://doi.org/10.1306/5d25c26d-16c1-11d7-8645000102c1865d>, 1967.

607 Jefferson, A., Grant, G. E., Lewis, S. L., and Lancaster, S. T.: Coevolution of hydrology and topography on a basalt
608 landscape in the Oregon Cascade Range, USA, *Earth Surf. Process. Landforms*, 35, 803–816,
609 <https://doi.org/10.1002/esp.1976>, 2010.

610 Karátson, D., Thouret, J. C., Moriya, I., and Lomoschitz, A.: Erosion calderas: Origins, processes, structural and
611 climatic control, *Bull. Volcanol.*, 61, 174–193, <https://doi.org/10.1007/s004450050270>, 1999.

612 Karátson, D., Telbisz, T., and Wörner, G.: Erosion rates and erosion patterns of Neogene to Quaternary
613 stratovolcanoes in the Western Cordillera of the Central Andes: An SRTM DEM based analysis, *Geomorphology*,
614 139–140, 122–135, <https://doi.org/10.1016/j.geomorph.2011.10.010>, 2012.

615 Kerr, R. C.: Thermal erosion by laminar lava flows, *J. Geophys. Res. B Solid Earth*, 106, 453–465,
616 <https://doi.org/10.1029/2001JB000227>, 2001.

617 Kirby, E. and Whipple, K. X.: Expression of active tectonics in erosional landscapes, *J. Struct. Geol.*, 44, 54–75,
618 <https://doi.org/10.1016/j.jsg.2012.07.009>, 2012.

619 Kirby, E., Whipple, K. X., Tang, W., and Chen, Z.: Distribution of active rock uplift along the eastern margin of the
620 Tibetan Plateau: Inferences from bedrock channel longitudinal profiles, *J. Geophys. Res. Solid Earth*, 108,
621 <https://doi.org/10.1029/2001JB000861>, 2003.

622 Lahitte, P., Samper, A., and Quidelleur, X.: DEM-based reconstruction of southern Basse-Terre volcanoes
623 (Guadeloupe archipelago, FWI): Contribution to the Lesser Antilles Arc construction rates and magma production,
624 *Geomorphology*, 136, 148–164, <https://doi.org/10.1016/j.geomorph.2011.04.008>, 2012.

625 Locke, C. A. and Cassidy, J.: Egmont Volcano, New Zealand: Three-dimensional structure and its implications for
626 evolution, *J. Volcanol. Geotherm. Res.*, 76, 149–161, [https://doi.org/10.1016/S0377-0273\(96\)00074-1](https://doi.org/10.1016/S0377-0273(96)00074-1), 1997.

627 Lohse, K. A. and Dietrich, W. E.: Contrasting effects of soil development on hydrological properties and flow paths,
628 *Water Resour. Res.*, 41, 1–17, <https://doi.org/10.1029/2004WR003403>, 2005.

629 Major, J. J., Mosbrucker, A. R., and Spicer, K. R.: Sediment erosion and delivery from Toutle River basin after the
630 1980 eruption of Mount St. Helens: A 30-year perspective, *Ecol. Responses Mt. St. Helens Revisit. 35 years after*
631 *1980 Erupt.*, 19–44, https://doi.org/10.1007/978-1-4939-7451-1_2, 2018.

632 McBirney, A. R., Serva, L., Guerra, M., and Connor, C. B.: Volcanic and seismic hazards at a proposed nuclear
633 power site in central Java, *J. Volcanol. Geotherm. Res.*, 126, 11–30, [https://doi.org/10.1016/S0377-0273\(03\)00114-](https://doi.org/10.1016/S0377-0273(03)00114-8)
634 8, 2003.

635 Mejía, A. I. and Niemann, J. D.: Identification and characterization of dendritic, parallel, pinnate, rectangular, and
636 trellis networks based on deviations from planform self-similarity, *J. Geophys. Res. Earth Surf.*, 113, 1–21,
637 <https://doi.org/10.1029/2007JF000781>, 2008.

638 Montgomery, D. R. and Dietrich, W. E.: Landscape Dissection and Drainage Area-Slope Threshold, in: *Process*
639 *Models and Theoretical Geomorphology*, 1994.

640 Mudd, S. M. and Furbish, D. J.: Responses of soil-mantled hillslopes to transient channel incision rates, *J. Geophys.*
641 *Res. Earth Surf.*, 112, 1–12, <https://doi.org/10.1029/2006JF000516>, 2007.

642 Mueller, J. E.: Re-evaluation of the relationship of master streams and drainage basins, *Bull. Geol. Soc. Am.*, 83,
643 3471–3474, [https://doi.org/10.1130/0016-7606\(1972\)83\[3471:ROTRROM\]2.0.CO;2](https://doi.org/10.1130/0016-7606(1972)83[3471:ROTRROM]2.0.CO;2), 1972.

644 Mulyaningsih, S. and Shaban, G.: Geochemistry of basaltic Merbabu volcanic rocks, Central Java, Indonesia,

- 645 Indones. J. Geosci., 7, 161–178, <https://doi.org/10.17014/ijog.7.2.161-178>, 2020.
- 646 O’Hara, D. and Karlstrom, L.: The arc-scale spatial distribution of volcano erosion implies coupled magmatism and
647 regional climate in the Cascades arc, United States, *Front. Earth Sci.*, 11, 1–15,
648 <https://doi.org/10.3389/feart.2023.1150760>, 2023.
- 649 O’Hara, D., Karlstrom, L., and Roering, J. J.: Distributed landscape response to localized uplift and the fragility of
650 steady states, *Earth Planet. Sci. Lett.*, 506, 243–254, <https://doi.org/10.1016/j.epsl.2018.11.006>, 2019.
- 651 O’Hara, D., Karlstrom, L., and Ramsey, D. W.: Time-evolving surface and subsurface signatures of Quaternary
652 volcanism in the Cascades arc, *Geology*, 49, e526, <https://doi.org/10.1130/g47706.1>, 2020.
- 653 Ollier, C.: *Volcanoes*, edited by: Blackwell, B., Oxford., 288 pp., 1988.
- 654 Perron, J. T. and Royden, L.: An integral approach to bedrock river profile analysis, *Earth Surf. Process. Landforms*,
655 38, 570–576, <https://doi.org/10.1002/esp.3302>, 2013.
- 656 Pierson, T. C. and Major, J. J.: Hydrogeomorphic effects of explosive volcanic eruptions on drainage basins, *Annu.*
657 *Rev. Earth Planet. Sci.*, 42, 469–507, <https://doi.org/10.1146/annurev-earth-060313-054913>, 2014.
- 658 Prince, P. S. and Spotila, J. A.: Evidence of transient topographic disequilibrium in a landward passive margin river
659 system: Knickpoints and paleo-landscapes of the New River basin, southern Appalachians, *Earth Surf. Process.*
660 *Landforms*, 38, 1685–1699, <https://doi.org/10.1002/esp.3406>, 2013.
- 661 Ricci, J., Lahitte, P., and Quidelleur, X.: Construction and destruction rates of volcanoes within tropical
662 environment: Examples from the Basse-Terre Island (Guadeloupe, Lesser Antilles), *Geomorphology*, 228, 597–607,
663 <https://doi.org/10.1016/j.geomorph.2014.10.002>, 2015.
- 664 Scherler, D. and Schwanghart, W.: Drainage divide networks - Part 1: Identification and ordering in digital elevation
665 models, *Earth Surf. Dyn.*, 8, 245–259, <https://doi.org/10.5194/esurf-8-245-2020>, 2020.
- 666 Schumm, S. A.: Evolution of drainage systems and slopes in badlands at Perth Amboy, New Jersey, *Bull. Geol. Soc.*
667 *Am.*, 67, 597–646, [https://doi.org/10.1130/0016-7606\(1956\)67\[597:EODSAS\]2.0.CO;2](https://doi.org/10.1130/0016-7606(1956)67[597:EODSAS]2.0.CO;2), 1956.
- 668 Schwanghart, W. and Scherler, D.: Short Communication: TopoToolbox 2 - MATLAB-based software for
669 topographic analysis and modeling in Earth surface sciences, *Earth Surf. Dyn.*, 2, 1–7, <https://doi.org/10.5194/esurf-2-1-2014>, 2014.
- 671 Shea, T. and van Wyk de Vries, B.: Structural analysis and analogue modeling of the kinematics and dynamics of
672 rockslide avalanches, *Geosphere*, 4, 657–686, <https://doi.org/10.1130/GES00131.1>, 2008.
- 673 Sklar, L. S. and Dietrich, W. E.: Sediment and rock strength controls on river incision into bedrock, *Geology*, 29,
674 1087–1090, [https://doi.org/10.1130/0091-7613\(2001\)029<1087:SARSCO>2.0.CO;2](https://doi.org/10.1130/0091-7613(2001)029<1087:SARSCO>2.0.CO;2), 2001.
- 675 Strahler, A. N.: Hypsometric (area-altitude) analysis of erosional topography, *Bull. Geol. Soc. Am.*, 63, 1117–1142,
676 <https://doi.org/10.1128/AAC.03728-14>, 1952.
- 677 Sweeney, K. E. and Roering, J. J.: Rapid fluvial incision of a late Holocene lava flow: Insights from LiDAR, alluvial
678 stratigraphy, and numerical modeling, *Bull. Geol. Soc. Am.*, 129, 500–512, <https://doi.org/10.1130/B31537.1>, 2017.
- 679 Talling, P. J., Stewart, M. D., Stark, C. P., Gupta, S., and Vincent, S. J.: Regular spacing of drainage outlets from
680 linear fault blocks, *Basin Res.*, 9, 275–302, <https://doi.org/10.1046/j.1365-2117.1997.00048.x>, 1997.
- 681 Thouret, J. C., Oehler, J. F., Gupta, A., Solikhin, A., and Procter, J. N.: Erosion and aggradation on persistently
682 active volcanoes—a case study from Semeru Volcano, Indonesia, *Bull. Volcanol.*, 76,
683 <https://doi.org/10.1007/s00445-014-0857-z>, 2014.
- 684 Ui, T. and Glicken, H.: Internal structural variations in a debris-avalanche deposit from ancestral Mount Shasta,
685 California, USA, *Bull. Volcanol.*, 48, 189–194, <https://doi.org/10.1007/BF01087673>, 1986.
- 686 van Wees, R. M. J., Tournigand, P.-Y., O’Hara, D., Grosse, P., Kereszturi, G., Campforts, B., Lahitte, P., and
687 Kervyn, M.: The role of erosion in the morphometry of composite volcanoes, in: EGU General Assembly

- 688 Conference Abstracts, EGU21-14500, 2021.
- 689 Wells, S. G., Dohrenwend, J. C., McFadden, L. D., Turrin, B. D., and Mahrer, K. D.: Late Cenozoic landscape
690 evolution on lava flow surfaces of the Cima volcanic field, Mojave Desert, California., *Geol. Soc. Am. Bull.*, 96,
691 1518–1529, [https://doi.org/10.1130/0016-7606\(1985\)96<1518:LCLEOL>2.0.CO;2](https://doi.org/10.1130/0016-7606(1985)96<1518:LCLEOL>2.0.CO;2), 1985.
- 692 Whipple, K. X., DiBiase, R. A., Ouimet, W. B., and Forte, A. M.: Preservation or piracy: Diagnosing low-relief,
693 high-elevation surface formation mechanisms, *Geology*, 45, 91–94, <https://doi.org/10.1130/G32501Y.1>, 2016.
- 694 Wicks, C. W., Dzurisin, D., Ingebritsen, S., Thatcher, W., Lu, Z., and Iverson, J.: Magmatic activity beneath the
695 quiescent Three Sisters volcanic center, central Oregon Cascade Range, USA, *Geophys. Res. Lett.*, 29, 26-1-26–4,
696 <https://doi.org/10.1029/2001GL014205>, 2002.
- 697 Willett, S. D., Slingerland, R., and Hovius, N.: Uplift, shortening, and steady state topography in active mountain
698 belts, *Am. J. Sci.*, 301, 455–485, <https://doi.org/10.2475/ajs.301.4-5.455>, 2001.
- 699 Willett, S. D., McCoy, S. W., Perron, T. J., Goren, L., and Chen, C. Y.: Dynamic reorganization of River Basins,
700 *Science (80-.)*, 343, <https://doi.org/10.1126/science.1248765>, 2014.
- 701 Yang, R., Willett, S. D., and Goren, L.: In situ low-relief landscape formation as a result of river network disruption,
702 *Nature*, 520, 526–529, <https://doi.org/10.1038/nature14354>, 2015.
- 703 Zernitz, E. R.: Drainage Patterns and Their Significance, *J. Geol.*, 40, 498–521, <https://doi.org/10.1086/623976>,
704 1932.
- 705